Toxicology and Applied Pharmacology 397 (2020) 115010

Contents lists available at ScienceDirect

Toxicology and Applied Pharmacology

journal homepage: www.elsevier.com/locate/taap

Mechanism underlying hooked resurgent-like tail currents induced by an insecticide in human cardiac Nav1.5

Sarah Thull[a], Cristian Neacsu[b], Andrias O. O'Reilly[c], Stefanie Bothe[a,d], Ralf Hausmann[e], Tobias Huth[b], Jannis Meents[a,1,2], Angelika Lampert[a,d,f,*,1]

[a] Institute of Physiology, RWTH Aachen University, Pauwelsstr. 30, 52074 Aachen, Germany
[b] Institut für Physiologie und Pathophysiologie, Friedrich-Alexander-Universität Erlangen-Nürnberg, Universitaetsstr. 17, 91054 Erlangen, Germany
[c] School of Natural Sciences and Psychology, Liverpool John Moores University, Liverpool, UK
[d] Research Training Group 2416 MultiSenses-MultiScales, RWTH Aachen University, Aachen, Germany
[e] Institute of Clinical Pharmacology, RWTH Aachen University, Wendlingweg 2, 52074 Aachen, Germany
[f] Research Training Group 2415 ME3T, RWTH Aachen University, Aachen, Germany

ARTICLE INFO

Keywords:
Voltage-gated sodium channel
Human Nav1.5
Sodium channel gating states
Resurgent current
Pyrethroid
Deltamethrin

ABSTRACT

Voltage-gated sodium channels are responsible not only for the fast upstroke of the action potential, but they also modify cellular excitability via persistent and resurgent currents. Insecticides act via permanently opening sodium channels to immobilize the animals. Cellular recordings performed decades ago revealed distinctly hooked tail currents induced by these compounds. Here, we applied the classical type-II pyrethroid deltamethrin on human cardiac Nav1.5 and observed resurgent-like currents at very negative potentials in the absence of any pore-blocker, which resemble those hooked tail currents. We show that deltamethrin dramatically slows both fast inactivation and deactivation of Nav1.5 and thereby induces large persistent currents. Using the sea anemone toxin ATx-II as a tool to prevent all inactivation-related processes, resurgent-like currents were eliminated while persistent currents were preserved. Our experiments suggest that, in deltamethrin-modified channels, recovery from inactivation occurs faster than delayed deactivation, opening a brief window for sodium influx and leading to hooked, resurgent-like currents, in the absence of an open channel blocker. Thus, we now explain with pharmacological methods the biophysical gating changes underlying the deltamethrin induced hooked tail currents.

Summary: The pyrethroid deltamethrin induces hooked resurgent-like tail currents in human cardiac voltage-gated Nav1.5 channels. Using deltamethrin and ATx-II, we identify additional conducting channel states caused by a faster recovery from inactivation compared to the deltamethrin-induced delayed deactivation.

1. Introduction

Voltage-gated sodium (Nav) channels consist of four homologous domains (DI – IV), each with six transmembrane segments (S1–6), that form the α-subunit (Ahern et al., 2016; Catterall, 2000). They are responsible for the fast upstroke of the action potential. The insecticide class of pyrethroids has been used abundantly since the 1970s, combatting agricultural pests and disease vectors, such as the malaria-transmitting *anopheles* mosquito (Field et al., 2017). Pyrethroids affect the function of insect Nav channels: They mostly act by slowing deactivation, thus keeping the channels open and disrupting the electrical communication of insect nerves and muscle cells (Soderlund, 2010, 2012). Already decades ago, these compounds were investigated in patch-clamp recordings and described to induce the so-called "hooked tail currents": during repolarization following a depolarizing voltage step the channels would reactivate, and thereby form a typical hook, instead of the normally visible single exponential decline of the tail currents (Tatebayashi and Narahashi, 1994; Song and Narahashi, 1996). It was speculated about the underlying molecular mechanism, but to date it was not resolved.

Following depolarization, Nav channels activate due to outward movement of the voltage-sensors of each domain (Chahine et al., 1994; Yang et al., 1996; Ahern, 2013). Milliseconds after activation, and after the four channel domains have moved to their outward position, the

* Corresponding author at: Institute of Physiology, RWTH Aachen University, Pauwelsstr. 30, 52074 Aachen, Germany.
E-mail addresses: jmeents@multichannelsystems.com (J. Meents), alampert@ukaachen.de (A. Lampert).
[1] shared corresponding authors.
[2] Present adress of J. Meents: Multi Channel Systems MCS GmbH, Aspenhaustrasse 21, 72770 Reutlingen, Germany.

https://doi.org/10.1016/j.taap.2020.115010
Received 10 February 2020; Received in revised form 12 April 2020; Accepted 14 April 2020
Available online 15 April 2020
0041-008X/

inactivation particle (located within the linker between DIII and DIV) binds to the open pore most likely from the transmembrane side, as suggested by an allosterical model (Yan et al., 2017; Pan et al., 2018; Rühlmann et al., 2019): this induces a conformational change which occludes the permeation pathway (Bezanilla and Armstrong, 1977; Armstrong, 1981; West et al., 1992; Catterall, 2000; Armstrong, 2006). During repolarization, the four activated domains return to their resting position, thus closing the channel pore and deactivating the channel (Kuo and Bean, 1994). Recent models of Nav channel gating suggest that activation of DI – III is sufficient for channel opening and current flux. DIV movement, albeit not required for channel opening, is responsible for initiating fast inactivation as it forms the docking site of the inactivation particle. Equally, the return of DIV to its resting position is required for the detachment of the inactivation particle and recovery of the channel from fast inactivation (Kuo and Bean, 1994; Armstrong, 2006; Capes et al., 2013; Ahern et al., 2016). Pyrethroids are mainly predicted to bind to DII and DIII S6 of the insect Nav channel (Vais et al., 2003; O'Reilly et al., 2006; Usherwood et al., 2007; Oliveira et al., 2013; Dong et al., 2014; Du et al., 2015), thus stabilizing the bound channel domain, most probably DII, in its activated conformation. Accordingly, deltamethrin has been shown to impair the transition of DII to its deactivated position (O'Reilly et al., 2006; Oliveira et al., 2013; Dong et al., 2014; O'Reilly et al., 2014; Du et al., 2015). Thus, deltamethrin mainly affects Nav channels by slowing of deactivation (Tabarean and Narahashi, 1998, 2001; Vais et al., 2000) but might also have a minor effect on fast inactivation (Chinn and Narahashi, 1986; He and Soderlund, 2016; James et al., 2017).

Although humans are less sensitive to pyrethroids, neurotoxic symptoms of pyrethroid intoxication have been described and are most likely mediated by Nav modification (Mowry et al., 2016; Field et al., 2017; James et al., 2017). They include T-syndrome (tremor) for type-I pyrethroids and CS-syndrome (choreoathetosis and salivation) for type-II pyrethroids, including deltamethrin. Besides these common neuronal symptoms after pyrethroid intoxication, some case studies of human deltamethrin intoxication report of chest tightness and palpitations, pointing towards potential cardiac side effects of the pyrethroid (He et al., 1989; Mowry et al., 2016).

Nine Nav channel α-subunits (Nav1.1–1.9) have been identified to date (Catterall, 2000; Ahern et al., 2016). The main Nav channel in cardiac tissue is Nav1.5 and mutations of this channel are known to cause cardiac diseases, such as long QT syndrome type 3, Brugada syndrome or sick sinus syndrome (Zaydman et al., 2012; Varga et al., 2015). Thus, deltamethrin at higher concentrations may induce Nav1.5-mediated cardiac side effects in humans.

One or two smaller auxiliary sodium channel β-subunits (β1–4) may be associated with one Nav channel α-subunit (Catterall, 2000, 2010), regulating different channel functions (Calhoun and Isom, 2014; Zhu et al., 2017). The β4-subunit is most likely involved in the generation of resurgent currents: during depolarization a positively charged intracellular pore-blocker, most likely the C-terminus of the β4-subunit (Lewis and Raman, 2014), may quickly enter and occlude the open pore. This open-channel block impairs fast inactivation. Unbinding of the pore-blocker upon repolarization generates the “resurgent current” (Raman and Bean, 1997; Lewis and Raman, 2014). This classical resurgent current is believed to promote high-frequency action potential firing (Raman and Bean, 1997, 2001) but is also linked to certain disease states e.g. paroxysmal extreme pain disorder (Jarecki et al., 2010; Hampl et al., 2016) or epilepsy (Hargus et al., 2013).

The sea anemone toxin ATx-II profoundly enhances persistent currents and classical resurgent currents induced by the β4-peptide (Klinger et al., 2012; Lewis and Raman, 2013). The toxin impairs fast inactivation by slowing the outward movement of DIV, keeping it in its resting position (el-Sherif et al., 1992; Warmke et al., 1997; Sheets et al., 1999; Vais et al., 2000; Stevens et al., 2011). These properties render this toxin a handy tool to study the involvement of DIV movement in sodium channel gating.

Using these tools, we here describe the molecular mechanism underlying hooked tail currents induced by pyrethroids: Deltamethrin provokes resurgent-like sodium currents at very negative potentials in the absence of an open channel blocker. Using both deltamethrin, which slows deactivation (e.g. of DII), and ATx-II, which slows activation of DIV, we identify an additional conducting sodium channel gating state that resembles resurgent currents, underlying the so-called “hooked tail currents”. We present a model that explains the effects of both compounds on Nav1.5 function and give evidence for an alternative way of resurgent current induction in sodium channels.

2. Experimental procedures

2.1. Cell culture and transfection

HEK293 cells, either stably expressing human Nav1.5 or used for transient transfection of Nav1.7, were maintained in DMEM / F-12 medium (Gibco-Life technologies) including 10% FBS, 1% Penicillin/Streptomycin (A&E Scientific). 0.1 mg/ml Zeocin (Thermo Fischer Scientific) was added to the medium for the HEK293 cell line stably expressing human Nav1.5. ND7/23 cells used for transient transfection with Nav1.8 were maintained in DMEM / F-12 medium (Gibco-Life technologies) with a higher glucose rate of 4.5 g/l, including 10% FBS. Cells were incubated at 37 °C and 5% CO_2.

Human Nav1.8 plasmid in a modified pIRESpuro3 vector (Kaluza et al., 2018) and human Nav1.7 plasmid in a pCMV6-neo vector (Klugbauer et al., 1995; Stadler et al., 2015) were transfected using JetPEI reagent (Polyplus Transfection, Illkirch, France): 1.375 µg Nav1.7 / Nav1.8 WT DNA was transfected to HEK293 cells for Nav1.7 and to ND7/23 cells for Nav1.8, using 3 µl of the JetPEI reagent. The channel constructs were cotransfected with 0.125 µg GFP to detect transfected cells via green fluorescence. Cells were recorded one day after transfection.

2.2. Chemicals

All chemicals were purchased from Sigma (Germany) or Merck (Germany) unless otherwise stated. A stock solution of the β4-peptide (sequence ‘KKLITFILKKTREK’, PSL GmbH), dissolved in water, was diluted in internal solution to a final concentration of 100 µM and kept at 4 °C until used for experiments.

Recombinant ATx-II (*Anemonia sulcata* toxin, Alomone Labs, Jerusalem, Israel or Sigma-Aldrich, USA), dissolved in water, was added to the bath solution to a final concentration of 5 nM. Deltamethrin (Sigma-Aldrich, USA), diluted in DMSO, was added to the bath solution to a final concentration of 1 µM. The final concentration of DMSO in extracellular solution for recordings of Nav1.5 did not exceed 0.1% or 0.2% for Nav1.7 and Nav1.8, which had no effect on sodium currents. In control recordings, cells were treated with a vehicle (0.1% DMSO, or 0.2% for Nav1.7 and Nav1.8) in bath solution, instead of deltamethrin or ATx-II. Cells treated with vehicle and HEK293 cells expressing Nav1.5 treated with deltamethrin were incubated for minimum 5 min before each recording in the same dish as they were patched. HEK293 cells transfected with Nav1.7 and ND7 cells transfected with Nav1.8 treated with deltamethrin were patched on coverslips coated with PDL (Poly-D-Lysine Hydrobromide (Sigma-Aldrich, USA)) and transferred to a dish pre-incubated with deltamethrin for minimum 5 min.

2.3. Electrophysiology

Whole-cell patch-clamp experiments on HEK293 cells, stably expressing human Nav1.5, were performed with an EPC-10USB amplifier (HEKA Elektronik, Lambrecht, Germany) at room temperature. Glass pipettes, manufactured with a DMZ puller (Zeitz Instruments GmbH, Martinsried, Germany) to a resistance of 0.9 to 2.5 MΩ were filled with internal solution containing (in mM): 140 CsF, 10 NaCl, 10 HEPES, 1

EGTA, 18 Sucrose (pH 7.33, adjusted with CsOH). For some experiments ß4-peptide was diluted in internal solution to a final concentration of 100 μM. The external bath solution contained (in mM): 140 NaCl, 3 KCl, 1 $MgCl_2$, 1 $CaCl_2$, 10 HEPES, 20 Glucose (pH 7.4, adjusted with NaOH).

Capacitive transients were cancelled and series resistance (≤5 MΩ, for measurements of the recovery of fast inactivation and for recordings with 10 μM deltamethrin ≤7 MΩ) was compensated by at least 65%. Leak current was subtracted online using the P/4 procedure following (Nav1.5) or preceeding (Nav1.7 and Nav1.8) the test pulse. Signals were digitized at sampling rates of 100 kHz for recordings of current-voltage relations, steady-state fast inactivation and deactivation and 50 kHz for recordings of resurgent current and recovery of fast inactivation. Low-pass filter frequency was set to 10 kHz. Voltage protocols were started 3 to 5 min after establishing the whole-cell configuration to allow for current stabilization. The holding potential was set to -120 mV, except for measurements of recovery of fast inactivation of Nav1.5 with deltamethrin, where a holding potential of -150 mV was used to avoid a time-dependent shift of fast inactivation (Meents, 2018). For acquisition and off-line analysis Patchmaster / Fitmaster software (HEKA Elektronik, Lamprecht, Germany) was used. Currents of activation, steady-state fast inactivation, decay of fast inactivation, deactivation and recovery of fast inactivation curves as well as persistent current were analyzed without leak subtraction to reduce the impact of deltamethrin-altered leak currents on Nav1.5 sodium currents. The above-mentioned currents were additionally analyzed without zero offset subtraction to include persistent current summation during protocol repetition.

Current-voltage (I−V) relations were obtained using 100 ms pulses to a range of test potentials in 10 mV steps at an interval of 5 s. The voltage-dependent sodium channel conductance G_{Na} was calculated using the following equation: $G_{Na} = I_{Na}/(V_m - V_{rev})$ where I_{Na} is the amplitude of the current at the voltage V_m, and V_{rev} is the reversal potential for sodium, which was determined for each cell individually. Conductance was normalized to the maximum conductance of each individual cell. Activation curves were then derived by plotting normalized conductance ($G_{Na}/G_{Na,max}$) as a function of test potential and fitted with the Boltzmann equation: $G_{Na}/G_{Na,max} = G_{Na,\ max}/(1 + \exp.[(V_m - V_{1/2})/k])$ where $G_{Na,\ max}$ is the maximum sodium conductance, $V_{1/2}$ is the membrane potential at half-maximal channel activation, V_m is the membrane voltage and k is the slope factor.

Mean persistent current was evaluated after the first 100 ms and during the final 10 ms of a 500 ms depolarizing pulse in a voltage range of -150 mV to +20 mV (in Fig. 4d) as well as during the final 13 ms of a 100 ms depolarizing pulse from -120 mV to +20 mV (see Fig. 2b (Thull et al., 2020)). Currents were normalized to the maximum current, elicited by the depolarizing pre-pulse.

Resurgent currents were assessed using a 20 ms depolarizing pre-pulse to 0 mV to allow channel opening, followed by a 500 ms test pulse in steps of 10 mV (ranging from −120 mV to +20 mV) with deltamethrin in the bath and in some experiments with the β4-peptide in the internal solution or ATx-II in the external solution. Currents measured with β4-peptide shown in Fig. 3d were assessed using a 20 ms depolarizing pre-pulse to +30 mV, followed by 500 ms test pulses ranging from -120 mV to +20 mV, as β4-resurgent currents enhance with increasing depolarizations. To measure even very small resurgent currents, currents were analyzed without leak subtraction. Absolute currents were analyzed by subtracting the maximum resurgent current from a baseline which was defined as shown in Fig. 2a. Resurgent currents were normalized to the maximum inward current, elicited by the depolarizing pre-pulse. Resurgent current kinetics was investigated by measuring the time-to-peak of the resurgent current at the beginning of the repolarizing pulse.

Voltage dependence of steady-state fast inactivation was measured using a series of 500 ms pre-pulses ranging from −150 mV to −10 mV in steps of 10 mV, followed by a 40 ms depolarization to +20 mV that served as a test pulse to assess the available non-inactivated channels. Normalized maximum inward current amplitude ($I_{Na}/I_{Na,\ Max}$) at each test pulse is displayed as a function of pre-pulse potential. Steady-state fast inactivation of vehicle recordings of Nav1.5 channels were fitted using the above Boltzmann equation, providing a measure of $V_{1/2}$ (the potential of half maximal inactivation).

For calculating the slow time course of persistent current decay, the above steady-state fast inactivation protocol was used to activate and inactivate channels. Only the slow component of current decay over 500 ms was fitted by a double-exponential equation (see Fig. 5a): $Y = Y_0 + A_{fast}*\exp.(-K_{fast}*X) + A_{slow}*\exp.(-K_{slow}*X)$, where Y_0 is the current amplitude at steady-state (i.e. plateau), A_{fast} and A_{slow} represent the amplitude coefficient for the fast and the slow time constants, K_{fast} and K_{slow} represent the two rate constants and X is the time. The time constants τ_{fast} and τ_{slow} are the reciprocals of the respective rate constant K.

For recovery experiments, channels were examined by using a 20 ms pre-pulse to −30 mV, followed by a repolarization to −110 mV for varying intervals (from 0.1 ms to 1638 ms) and a test-pulse to −30 mV to determine the fraction of recovered channels. Test-pulse currents were normalized to the corresponding pre-pulse currents and plotted against recovery interval. The time constant of recovery of fast inactivation, given as τ, was calculated by fitting the data with a double-exponential equation as described above.

For deactivation experiments, channels were examined by using a 0.4 ms depolarizing pre-pulse to +20 mV, followed by a repolarization from −120 mV to +20 mV in 10 mV steps. For calculating the slow time course of persistent current decay at deactivating voltages, the slow component of tail current decay over 100 ms was fitted by the above double-exponential equation (see Fig. 5b).

2.4. Data analysis and statistics

Data were analyzed and graphed using Fitmaster software (HEKA Elektronik), Igor Pro 5.2 and 6.3 software (Wavemetrics), Graphpad Prism 5, 6, 7 or 8 (GraphPad Software) and Corel Draw X3–X6 (Corel Corporation). Data are presented as mean ± SEM.

For statistical testing, more than two groups were compared by an ANOVA or a Kruskal-Wallis test in case of non-Gaussian distribution, followed by a Bonferroni, Dunnett or Dunn post-hoc analysis. Two groups were compared with a student's *t*-test for parametric testing or a Mann Whitney test for non-parametric testing and significance was assumed if $p \leq .05$. We specified the significance level by the 95% confidence interval, the difference between the means and t-ratio (difference between sample means divided by the standard error of the difference) for parametric testing or the actual difference between medians and the 95.10%, 95.69% or 95.74% confidence interval (see Fig. 2 (Thull et al., 2020)) for non-parametric testing. Exponential fits and area under the curve (AUC) data were tested for significant outliers with Grubb's test (Graph pad QuickCalcs) and significant outliers were excluded from analysis.

3. Results

3.1. Deltamethrin induces resurgent-like currents without open-channel pore-blocker

Nav channels may produce resurgent currents that are usually induced by an open-channel pore-blocker such as the β4-peptide that unbinds during repolarization (Raman and Bean, 1997). Previous reports suggest that pyrethroids induce hooked tail currents (Tatebayashi and Narahashi, 1994; Song and Narahashi, 1996), and we tested whether deltamethrin has this effect on the neuronal sodium channels Nav1.7 and Nav1.8 and the cardiac sodium channel Nav1.5. Indeed, following incubation with 1 μM deltamethrin, we observed hooked tail currents during a repolarization to −120 mV in all three channel

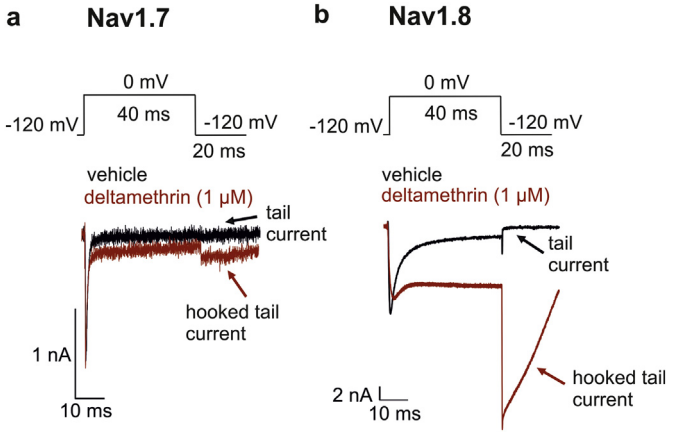

Fig. 1. Hooked sodium tail currents in Nav1.7 and Nav1.8 channels. (a) Nav1.7 channels transiently transfected into HEK293 cells. Representative current traces evoked by the indicated voltage protocol. Cells were treated with vehicle (black) and 1 μM deltamethrin (red) (b) Nav1.8 channels transiently transfected into ND7/23 cells. Representative current traces evoked by the indicated voltage protocol. Cells were treated with vehicle (black) and 1 μM deltamethrin (red).
The black arrow indicates tail currents of Nav1.7 or Nav1.8 treated with vehicle whereas the red arrow displays hooked tail currents induced by deltamethrin in Nav1.7 or Nav1.8 channels. (For interpretation of the references to colour in this figure legend, the reader is referred to the web version of this article.)

isoforms (Fig. 1a, b and Fig. 2a, b). Nav1.7's sodium tail currents and their hook elicited by deltamethrin were small and hard to investigate (Fig. 1a), which is expected as mammalian Nav1.7 is regarded as pyrethroid resistant (Tan and Soderlund, 2011). Hooked Nav1.8 tail currents induced by deltamethrin merged almost immediately into large and slow tail currents due to the slow gating properties of these channels and thus, complicated a decent analysis of the hooked tail currents (Fig. 1b). We focused on investigating the hooked tail current component of Nav1.5 channels, as they are gating fast and evoke tail currents that were large enough and suitable for evaluating their hook and its underlying mechanism appropriately.

When recording fast gating Nav1.5 channels treated with 1 μM deltamethrin, we unexpectedly observed small hooked tail currents that resembled resurgent currents known from Nav channels in the central nervous system (Raman and Bean, 1997). Unlike typical resurgent currents, however, these resurgent-like currents of Nav1.5 were induced in the absence of an open-channel pore-blocker (Fig. 2a, b) and did not increase with higher concentrations of deltamethrin (see Fig. 1 (Thull et al., 2020)). They merged quickly into large deltamethrin-induced persistent currents and were observed only at very negative voltages (between −120 mV and − 90 mV). Compared to tail currents, which decay exponentially directly after repolarization, deltamethrin-induced hooked, resurgent-like currents showed a clearly detectable activation component and a relatively slow time-to-peak (Fig. 3).

We investigated the effect of β4-peptide on Nav1.5 channels with and without deltamethrin incubation in order to examine possible functional interactions between deltamethrin and β4-peptide. β4-induced resurgent currents arose between −60 mV and − 30 mV (Fig. 3a, b). Deltamethrin-induced hooked, resurgent-like currents, on the other hand, had a different voltage dependence (between −120 mV and − 90 mV, Fig. 2b), were approximately tenfold smaller (compare Fig. 2b and 3b) and slower to reach their peak (Fig. 3d) than those mediated by β4. These data indicate that β4-peptide and deltamethrin generate resurgent currents by distinct underlying processes.

Combining both, deltamethrin and β4-peptide, resulted in approximately tenfold larger hooked, resurgent-like currents than those produced by deltamethrin alone (Fig. 3c). Interestingly, these currents now occurred almost over the entire voltage range from −120 mV to −10 mV, thus being a combination of deltamethrin and β4-induced resurgent currents. When compared to the effect of deltamethrin alone, currents induced by the combination of both compounds were slower to reach their peak (Fig. 3d). These findings support the idea that two different mechanisms of deltamethrin and β4-peptide exist and can work synergistically to induce resurgent currents.

3.2. Deltamethrin produces persistent current

We investigated if deltamethrin affects voltage sensitivity of activation and fast inactivation of Nav1.5. First, using a stepwise depolarization protocol (Fig. 4a), we found that 1 μM deltamethrin did not significantly shift the activation midpoint of Nav1.5 in a hyperpolarized direction (Fig. 4a, b). Next, using a two-pulse protocol (Fig. 4c) we found that steady-state fast inactivation of deltamethrin and of vehicle measurements of Nav1.5 channels were identical (Fig. 4d), indicating that the voltage dependence of steady-state fast inactivation is not affected by 1 μM deltamethrin. However, Nav1.5 channels treated with deltamethrin showed an unusual increase in relative current between −70 mV to −10 mV (Fig. 4d). This increase seemed to correlate with a

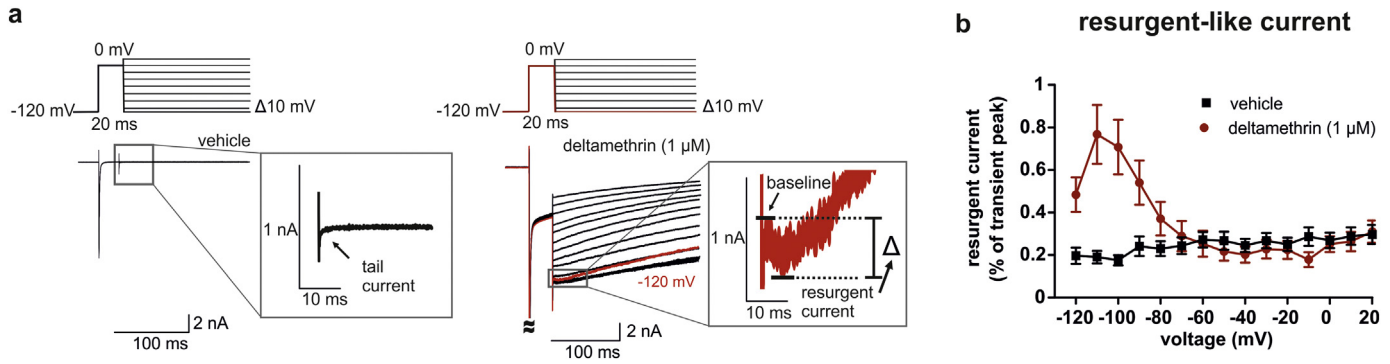

Fig. 2. Nav1.5 channels display resurgent-like currents.
(a) Representative current traces evoked by the indicated voltage protocol in human Nav1.5 channels stably expressed in HEK293 cells. Cells were treated with vehicle (left, black) and 1 μM deltamethrin (right, red). Magnified sections show the tail current in vehicle recordings and a resurgent-like current at −120 mV of 1 μM deltamethrin. Resurgent-like currents were determined as maximal current, elicited during repolarization, subtracted from a baseline. (b) Resurgent-like currents were normalized to maximum inward current of the depolarizing pre-pulse. Maximum resurgent-like currents were obtained at −110 mV: 1 μM deltamethrin 0.77% ± 0.13% (red, n = 15, mean AUC (−120 mV to −80 mV) 0.02 mV% ± 0.003 mV%), vehicle 0.19% ± 0.03% (black, n = 15, mean AUC (−120 mV to −80 mV) 0.01 mV% ± 0.002 mV%, p = .0005 vs. vehicle, difference between means = 0.01 mV% ± 0.003 mV%, 95% CI 0.006 mV% to 0.02 mV%, t-ratio = 3.9, unpaired t-test of the area under the curve (AUC) (−120 mV to −80 mV)). (For interpretation of the references to colour in this figure legend, the reader is referred to the web version of this article.)

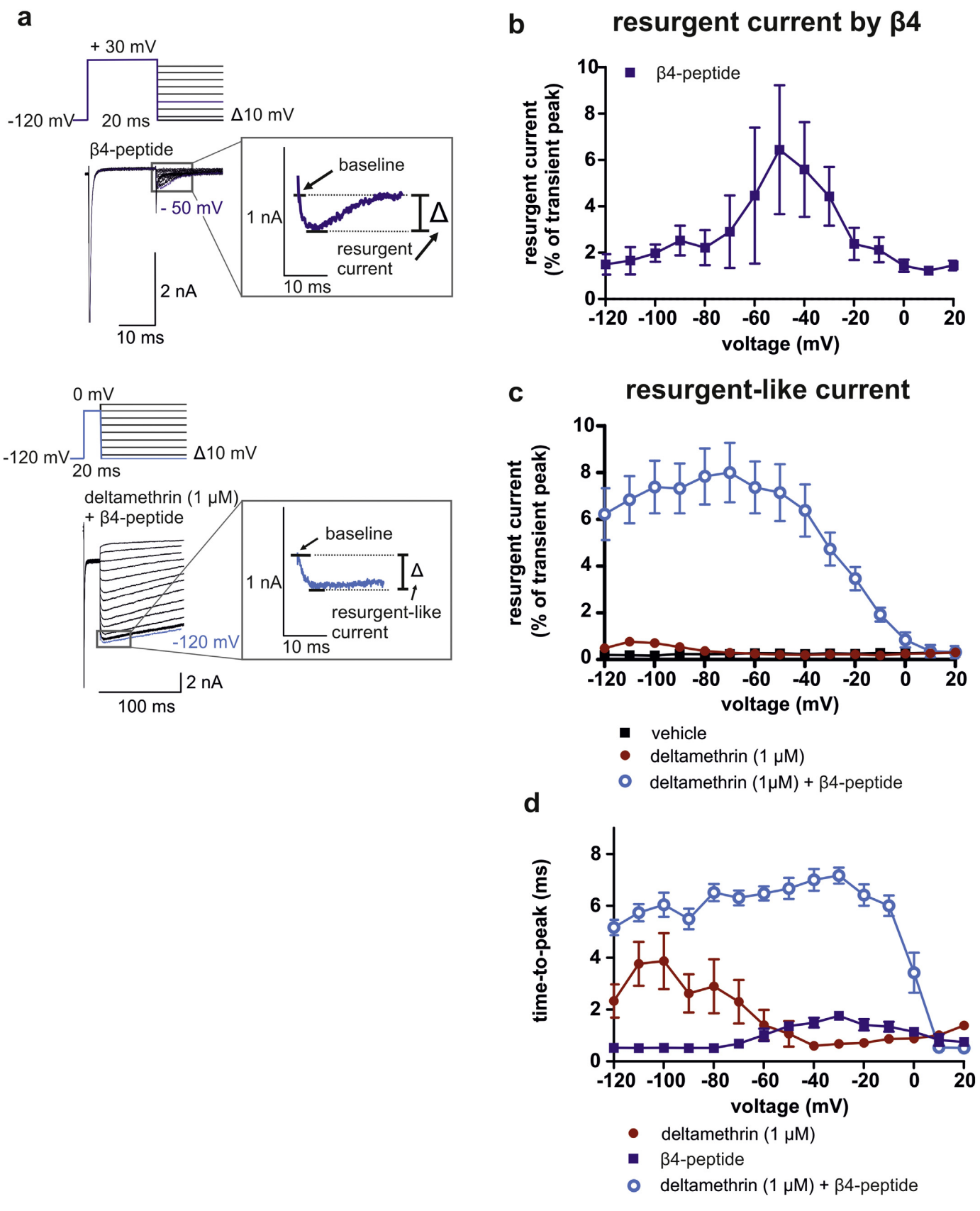

(caption on next page)

prominent persistent current, which we set out to analyze in more detail.

Nav channels affected by deltamethrin are known to produce a continuous, persistent sodium inward current that still flows after hundreds of milliseconds (James et al., 2017). While Nav1.5 channels did not show any persistent current in vehicle measurements,

Fig. 3. Deltamethrin and β4-peptide generate resurgent(−like) currents by distinct mechanisms.
(a) Representative current traces evoked by the indicated voltage protocols in human Nav1.5 channels expressed in HEK293 cells. Cells were treated with 100 μM β4-peptide (top) and 1 μM deltamethrin +100 μM β4-peptide (bottom). Magnified sections show representative traces of resurgent current at −50 mV with β4-peptide (top; dark blue) and at −120 mV with 1 μM deltamethrin +100 μM β4-peptide (bottom; light blue). Resurgent-like currents were determined as in Fig. 2. (b) β4-mediated resurgent currents, evoked and analyzed as in (a), using a pre-pulse to +30 mV. The intracellular recording solution contained 100 μM β4-peptide. Resurgent currents were normalized as described in Fig. 2b. The maximum resurgent current was obtained at −50 mV (6.44% ± 3.78%; $n = 8$). Resurgent currents induced by the β4-peptide are much larger than deltamethrin-induced currents. Also note the different voltage dependence of β4 resurgent currents. (c) Resurgent-like currents, evoked by vehicle (black, $n = 16$), 1 μM deltamethrin (red, n = 16) or 1 μM deltamethrin +100 μM β4 peptide (blue, $n = 13$) as in (a), using a pre-pulse to 0 mV. The red and black graphs are the same as in Fig. 2b and were included for comparison. In contrast to individual deltamethrin and β4 peptide treatments, resurgent-like currents induced by the combination of both compounds are larger, appearing almost over the entire voltage range. (d) Time-to-peak of the resurgent-like current in the different treatments. Resurgent-like currents induced by deltamethrin are generally slower compared to β4 resurgent currents. The combination of both compounds increases the time-to-peak even further at most voltages. (For interpretation of the references to colour in this figure legend, the reader is referred to the web version of this article.)

deltamethrin-treated channels displayed large persistent currents (Fig. 4a, c). However, these recordings also displayed a quickly inactivating current component within the first milliseconds of depolarization. Thus, deltamethrin recordings seem to expose two differently acting fractions of channels. The voltage dependence of persistent currents is displayed in Fig. 4d. These currents only appear above −80 mV, which is the threshold of channel opening (Fig. 4b), and reached up to 68% of transient current amplitude after 100 ms of

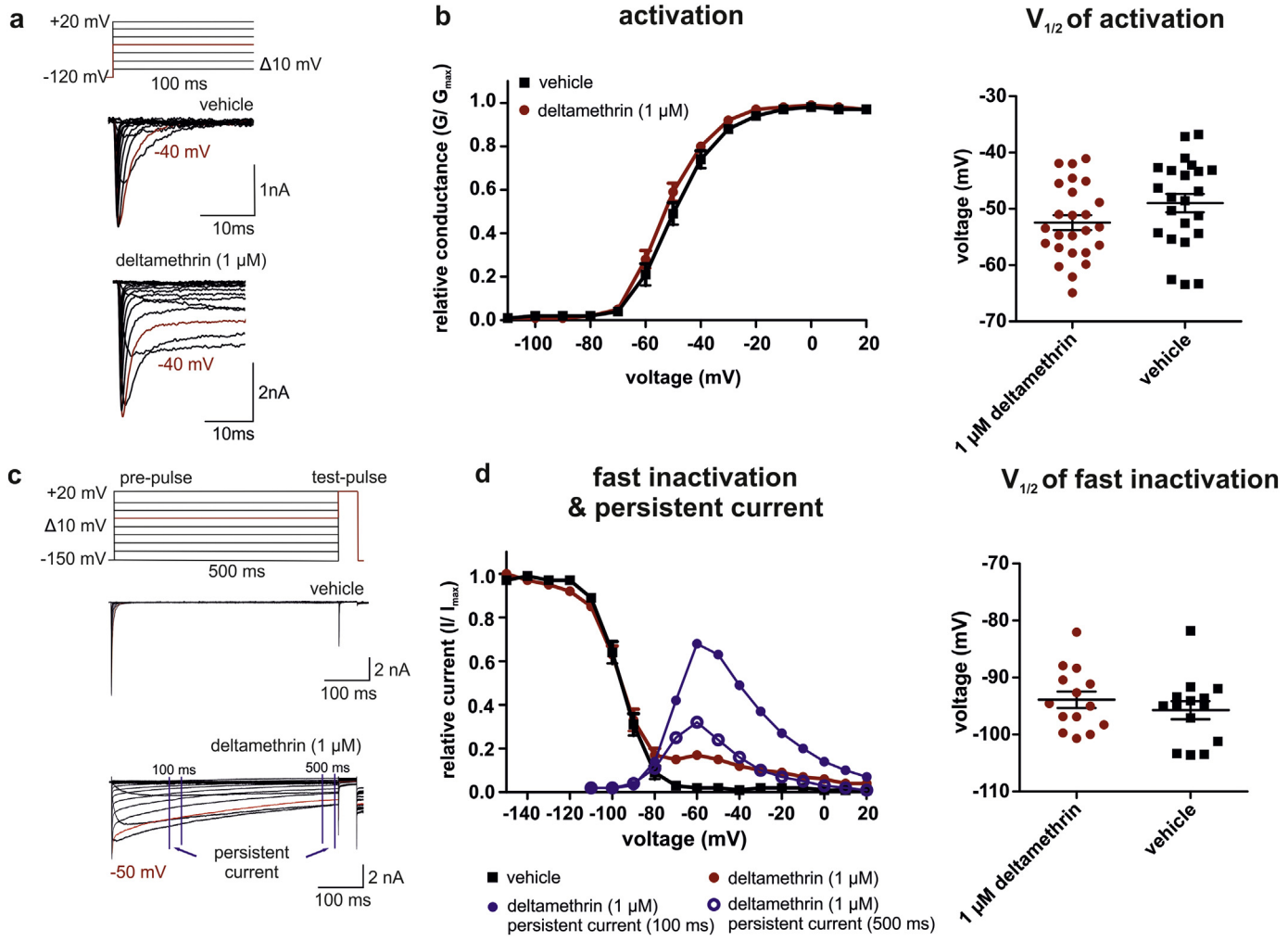

Fig. 4. Deltamethrin does not affect the voltage dependence of activation and fast inactivation of Nav1.5.
(a) Representative voltage protocol and current traces of activating sodium currents in vehicle or 1 μM deltamethrin recordings of human Nav1.5 in HEK293 cells. (b) Conductance-voltage relationship of Nav1.5 in vehicle or 1 μM deltamethrin. Values for half maximal voltage-dependent activation ($V_{1/2}$) obtained from Boltzmann fits are: 1 μM deltamethrin −52.5 mV ± 1.3 mV (red, $n = 14$); vehicle −49.0 mV ± 1.6 mV (black, n = 14, $p = .1$ vs. deltamethrin, difference between means = 3.5 mV ± 2.1 mV, 95% CI -0.7 mV to 7.7 mV, t-ratio = 1.7, unpaired t-test). (c) Representative voltage protocol and current traces of inactivating sodium currents in vehicle or 1 μM deltamethrin recordings of human Nav1.5 in HEK293 cells. (d) Voltage dependence of steady-state fast inactivation measured using the voltage protocol in (c). Half-maximal inactivation ($V_{1/2}$) of vehicle recordings: −95.7 mV ± 1.6 mV (black, n = 14), and of 1 μM deltamethrin recordings: −93.9 mV ± 1.5 mV (red, n = 14, $p = .4$ vs. vehicle, difference between means = 1.8 mV ± 2.4 mV, 95% CI -2.6 mV to 6.2 mV, t-ratio = 0.9, unpaired t-test). Half-maximal inactivation of deltamethrin recordings shows no difference to vehicle recordings. Mean persistent current of 1 μM deltamethrin recordings was measured after 100 ms (filled blue, n = 16) and after 500 ms of depolarizing pre-pulse (unfilled blue, n = 16). (For interpretation of the references to colour in this figure legend, the reader is referred to the web version of this article.)

depolarization, decreasing to 32% of transient current amplitude after 500 ms of depolarization (Fig. 4d). This indicates that persistent currents have a very slow time course and that channels only fully recover within the range of seconds.

In summary, the above data show that a fraction of channels seems to undergo regular gating and appears to be unaffected by deltamethrin. These channels are presumably unbound by the insecticide. Persistent current on the other hand seems to occur when a channel has bound deltamethrin. These channels remain continuously permeable to sodium ions and hence escape analysis to some extent due to their extremely altered gating kinetics. Deltamethrin presumably slows the time constants of fast inactivation and of deactivation and increases the likelihood to adopt an open state. Next, we therefore investigated the extremely slow time course of persistent currents and the effect of deltamethrin on channel inactivation and deactivation kinetics.

3.3. Deltamethrin slows fast inactivation and deactivation of a deltamethrin-bound Nav1.5 channel fraction

It has previously been suggested that deltamethrin mainly alters the deactivation process of Nav channels (Tabarean and Narahashi, 1998, 2001; Vais et al., 2000). Accordingly, when applying a voltage protocol for deactivation, we find large persistent currents even at very negative membrane potentials (Fig. 5b, c). However, the large persistent currents that we observed during protocols for fast inactivation (Fig. 4c), also suggest an effect of the compound on fast inactivation kinetics. Here, we tried to quantify the slowing of inactivation and deactivation kinetics by deltamethrin.

First, we investigated gating kinetics of the presumably unbound channel fraction using protocols for fast inactivation or channel deactivation (see Fig. 2 (Thull et al., 2020)). As expected, the fast time constants of both gating mechanisms were unaltered in this channel fraction.

In order to investigate the very slow time course of persistent current decay and thereby the deltamethrin-bound channels, we excluded the fast gating current component from our analysis and only fit the slow persistent current with a double exponential function. This analysis could only be performed in deltamethrin recordings, not in vehicle measurements, as the latter did not display any persistent current that could be fitted. Persistent currents in fast inactivation protocols decayed with slow time constants in the range of 200–400 ms (Fig. 5a), which corresponds with our earlier findings that 32% channels are still conductive after 500 ms of depolarization (Fig. 4c, d). When we measured channel deactivation, we found that deltamethrin-bound channels only deactivated with a very slow time constant in the range of 100–200 ms, resulting in very slowly inactivating persistent currents (Fig. 5b). After 100 ms, 9% of channels are still conductive even at −120 mV (Fig. 5c). These data demonstrate that deltamethrin slows both fast inactivation and deactivation of Nav1.5 channels and that these channels need hundreds of milliseconds to recover from the compound even at resting voltages. However, it is not yet clear how the slowed deactivation and inactivation can lead to the hooked, resurgent-like currents observed under deltamethrin treatment.

3.4. Deltamethrin does not alter recovery of fast inactivation

In the case of conventional resurgent currents, the β4-peptide blocks the open channel upon depolarization while competing with the fast inactivation particle. Consequently, it prevents fast inactivation (Raman and Bean, 2001; Lewis and Raman, 2014). So far, we have shown that deltamethrin generates hooked, resurgent-like currents by a different mechanism than the β4-peptide (different voltage dependence, see Fig. 3), presumably by affecting channel gating kinetics.

Here, we investigated if deltamethrin affects the recovery from fast inactivation of Nav1.5. If recovery was unaffected while deactivation was extremely slowed, channels might become conductive again during repolarization before deactivating, thus producing small hooked, resurgent-like currents. We chose a recovery potential of −110 mV as we observed the largest resurgent-like currents at that voltage (Fig. 2b). Data were best fitted with a double-exponential equation and both fast and slow recovery rates (τ_{fast} and τ_{slow}) were unaffected by deltamethrin treatment (Fig. 5d, e). It should be noted, however, that approximately 48% of Nav1.5 channels produced a persistent current that impeded analysis at very short recovery intervals below 10 ms (Fig. 5d, inset). In conclusion, 1 μM deltamethrin does not appear to have an impact on the recovery of fast inactivation kinetics of Nav1.5 channels. This agrees with the fact that deltamethrin most likely binds to DII whereas recovery from fast inactivation is mediated by DIV movement (see Discussion).

3.5. ATx-II prevents resurgent-like currents caused by deltamethrin

So far, we have shown that deltamethrin slows deactivation and fast inactivation of Nav1.5 to produce large persistent currents. At the same time, recovery from fast inactivation seems unaffected and this might explain the observed hooked, resurgent-like currents. To confirm that the process of fast inactivation is indeed necessary for resurgent-like currents, we chose the sea anemone toxin ATx-II as a tool to completely abolish fast inactivation (el-Sherif et al., 1992; Lewis and Raman, 2013). ATx-II is believed to stabilize DIV in its deactivated position, thus the inactivation-particle binding site is not formed, and the toxin thereby impedes fast inactivation (el-Sherif et al., 1992; Warmke et al., 1997; Vais et al., 2000). If fast inactivation is necessary for the hooked, resurgent-like currents induced by deltamethrin, then ATx-II should prevent them.

The voltage dependence of Nav1.5 channel activation when treated with 0.5 nM ATx-II and 1 μM deltamethrin was similar to that recorded from untreated cells (see Fig. 3b (Thull et al., 2020)). In comparison to deltamethrin alone, the combination of ATx-II and deltamethrin produced smaller persistent currents but with the same voltage dependence (see Fig. 3c (Thull et al., 2020)). On the other hand, the combination of ATx-II and β4-peptide induced smaller persistent currents with a different voltage dependence (see Fig. 3c (Thull et al., 2020)). This is consistent with different underlying mechanisms: while ATx-II only inhibits fast inactivation, deltamethrin mainly inhibits deactivation, which occurs at much more negative potentials.

The reduced persistent currents suggest that ATx-II can reduce the effect of deltamethrin on Nav1.5 gating. Accordingly, the combination of ATx-II and deltamethrin eliminated resurgent-like current induction entirely, exclusively eliciting tail currents (Fig. 6a, b). It should be noted that binding sites for deltamethrin and ATx-II do not overlap (Rogers et al., 1996; Vais et al., 2003; O'Reilly et al., 2014), so a block of the deltamethrin binding site by ATx-II is unlikely (see Discussion). This suggests that resurgent-like currents induced by deltamethrin indeed depend on functional fast inactivation, which is impaired by ATx-II.

4. Discussion

The present study characterizes the effects of deltamethrin on human Nav1.5 channels. We show that the pyrethroid slows deactivation and fast inactivation and stabilizes open channel states, not only leading to persistent current but also to hooked, resurgent-like currents.

In order to explain these unusual currents, we propose a simplified Nav channel gating model (Fig. 7), which is based on previous models (Kuo and Bean, 1994; Armstrong, 2006; Goldschen-Ohm et al., 2013). The model visualizes the movement of the four Nav channel domains (DI to DIV) during channel activation, inactivation and deactivation. During depolarization, in the absence of any compound, Nav channel domains DI, DII and DIII quickly change their conformation to the outward position and activate successively. DIII moves first, followed simultaneously by DI and DII, leading to opening of the channel pore (Fig. 7 a, C1 – C4) (Chanda and Bezanilla, 2002; Armstrong, 2006). DIV

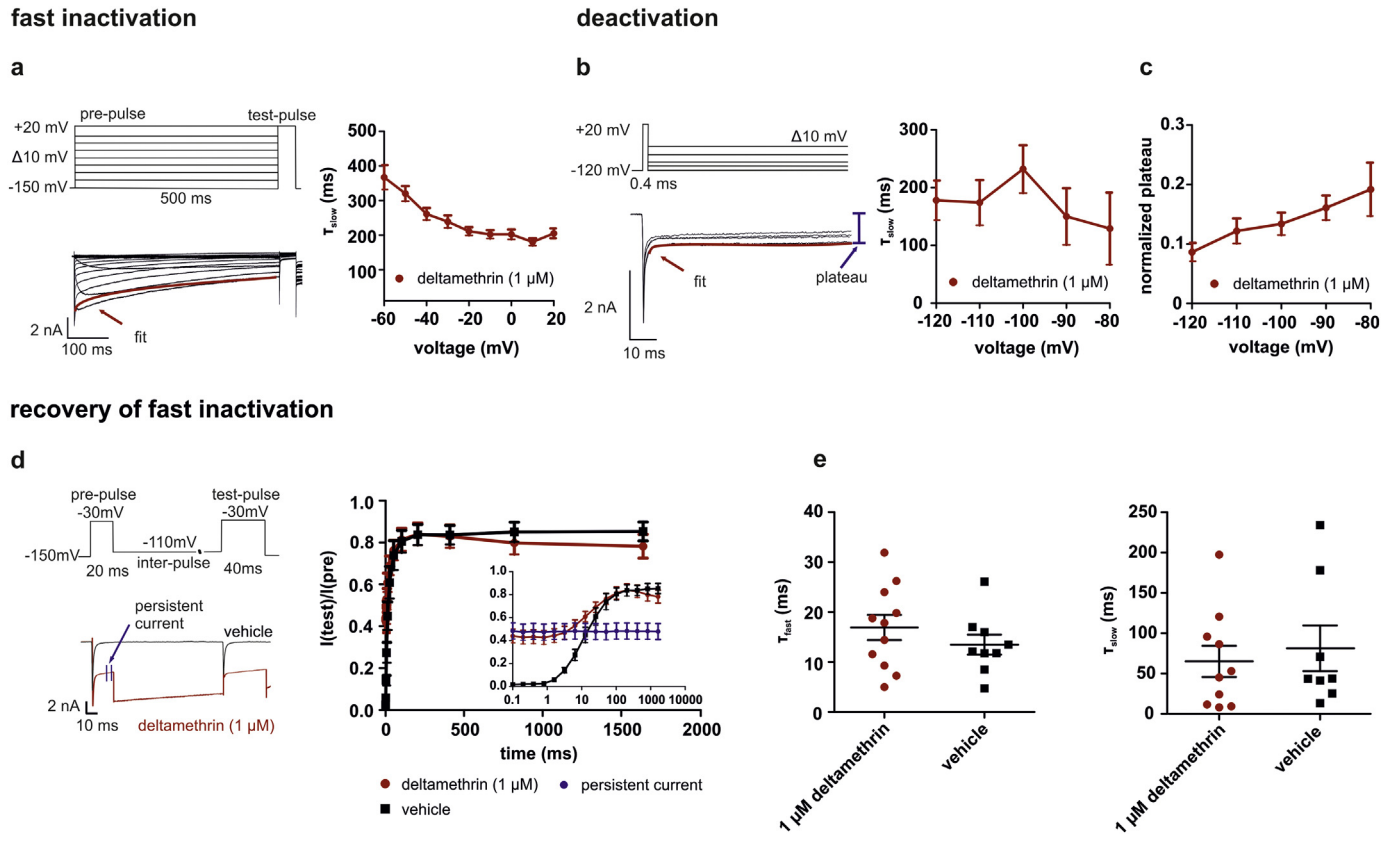

Fig. 5. Deltamethrin slows fast inactivation and deactivation but does not affect recovery of fast inactivation of Nav1.5 channels.
(a) Time course of persistent current decay during fast inactivation. Left: representative voltage protocol and traces of fast inactivation during 1 μM deltamethrin recordings. For calculating the slow time course of persistent current decay, time constants were obtained by a double-exponential fit to the slow component of current decay over 500 ms (fit highlighted in red). The quickly inactivating component (see Fig. 2 (Thull et al., 2020)) was not included in the fit. Right: slow time constant (τ_{slow}; n = 16) of persistent current decay. The fast time constant (τ_{fast}) is not displayed as it presumably represents a mixed population of deltamethrin bound and unbound channels. (b) Time course of persistent current decay during deactivation. Left: representative voltage protocol and traces of deactivation during 1 μM deltamethrin recordings. Calculating the time course of persistent current decay was performed as described in (a) but fitting over 100 ms (fit highlighted in red). Right: slow time constant (τ_{slow}; n = 19) of persistent current decay at deactivating voltages. (c) The fraction of persistent current remaining after 100 ms of deactivation was determined by the plateau of the double-exponential fit (blue arrow in b and Y_0 in function, see Methods). The plateau was normalized to the maximum tail current. (d) Recovery of fast inactivation during vehicle (black) and 1 μM deltamethrin (red) treatment was measured by the indicated voltage protocol with varying inter-pulse durations. Test-pulse current (I(test)) was normalized to the corresponding pre-pulse current (I(pre)) and plotted against inter-pulse duration. Data were best fitted with a double-exponential function and either depicted using a linear scale (right graph) or a logarithmic scale (inset). Mean persistent current (inset, n = 11) is shown in blue. Below 10 ms inter-pulse duration, persistent current prevents analysis of recovery. (e) Time course of recovery of fast inactivation represented by τ_{fast}: vehicle 13.5 ms ± 2.0 ms (black, n = 9) and 1 μM deltamethrin 16.9 ms ± 2.5 ms (red, n = 11, p = .3, difference between means = 3.4 ms ± 3.3 ms, 95% CI -3.6 ms to 10.4 ms, t-ratio = 1.0, no difference vs. vehicle, unpaired t-test); and by τ_{slow}: vehicle 81.3 ms ± 28.3 ms (black, n = 9) and 1 μM deltamethrin 65.1 ms ± 19.3 ms (red, n = 9, p = .6, difference between means = 16.2 ms ± 33.2 ms, 95% CI -54.2 ms to 86.6 ms, t-ratio = 0.5, no difference vs. vehicle, unpaired t-test). Deltamethrin does not affect the time courses of recovery from fast inactivation. (For interpretation of the references to colour in this figure legend, the reader is referred to the web version of this article.)

moves last to complete voltage sensor movement (Fig. 7a, C4 to O). This last step allows the inactivation particle (IFM motif within DIII –IV linker) to block the open channel pore (Fig. 7a, I) (Bezanilla and Armstrong, 1977; West et al., 1992; Capes et al., 2013; Ahern et al., 2016). During repolarization of the cell membrane, the activated Nav channel domains DI and DII quickly return to their resting position, followed by DIII and DIV, thus, deactivating the channel (Fig. 7a, CI3 – CI1) (Armstrong, 2006). Transition from state CI1 to state C1 involves the deactivation of DIV which finally allows the inactivation particle to unbind from the channel pore (Goldschen-Ohm et al., 2013). For the channel to be non-conductive, we assume that the channel pore either has to be blocked by the inactivation particle (Fig. 7a, I - CI1) or at least one of the domains DI to DIII have to be in their deactivated resting position (Fig. 7a, C1 – C3) (Xiao et al., 2014). Accordingly, the only conducting channel states are C4 and O.

4.1. Deltamethrin effect on Nav1.5 channel state properties

Deltamethrin is supposed to bind to open states with a higher affinity (O'Reilly et al., 2006; McCavera and Soderlund, 2012). Still, it is known to marginally modify resting Nav channel states (Tan and Soderlund, 2010; James et al., 2017). Since the binding site for deltamethrin is predicted to be located at DII (DII S4-S5 linker, DII S5 and DII S6) (O'Reilly et al., 2006, 2014), we assume that deltamethrin mainly stabilizes DII in its activated position. When DII remains activated, the two activated states C3 and C4 become equivalent (Fig. 7b, $C3/C4_d$). Complete channel deactivation must be slowed if DII remains in its activated conformation. Indeed, our recordings show a slowed time constant of deactivation due to deltamethrin. Thus, our data correspond well with previous findings in insect and mammalian sodium channels and underline that deltamethrin slows channel deactivation (Tabarean and Narahashi, 1998; Vais et al., 2000; Tabarean and Narahashi, 2001). However, we also show a slowing of fast inactivation

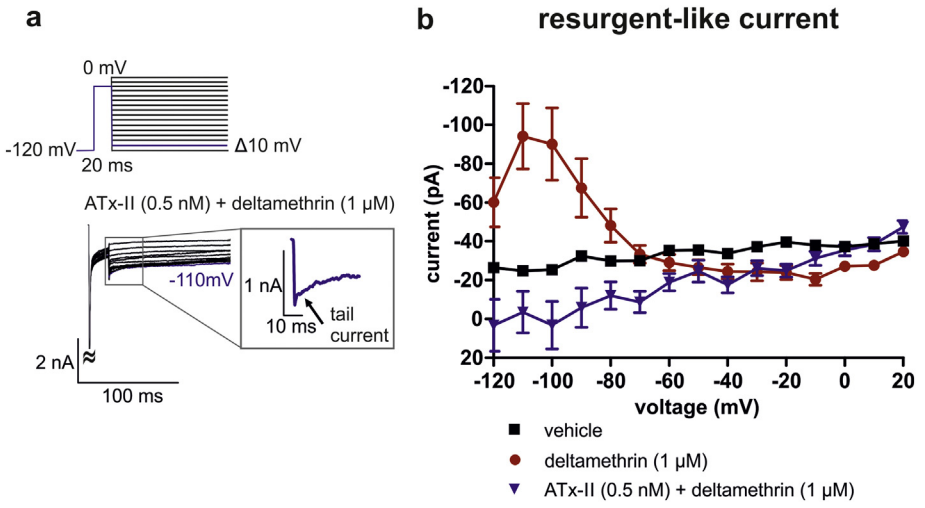

Fig. 6. ATx-II prevents the generation of resurgent-like currents.
(a) Representative currents evoked by the indicated voltage protocol in 0.5 nM ATx-II + 1 μM deltamethrin. The highlighted trace is magnified in the grey box, showing tail currents but no resurgent-like currents. (b) Resurgent-like currents, determined as described in Fig. 2a, during vehicle (black, n = 22), 1 μM deltamethrin (red, n = 19) or 1 μM deltamethrin +0.5 nM ATx-II (blue, n = 11). To simplify comparison, the y-axis is inverted. The combination of ATx-II and deltamethrin does not generate resurgent-like currents. (For interpretation of the references to colour in this figure legend, the reader is referred to the web version of this article.)

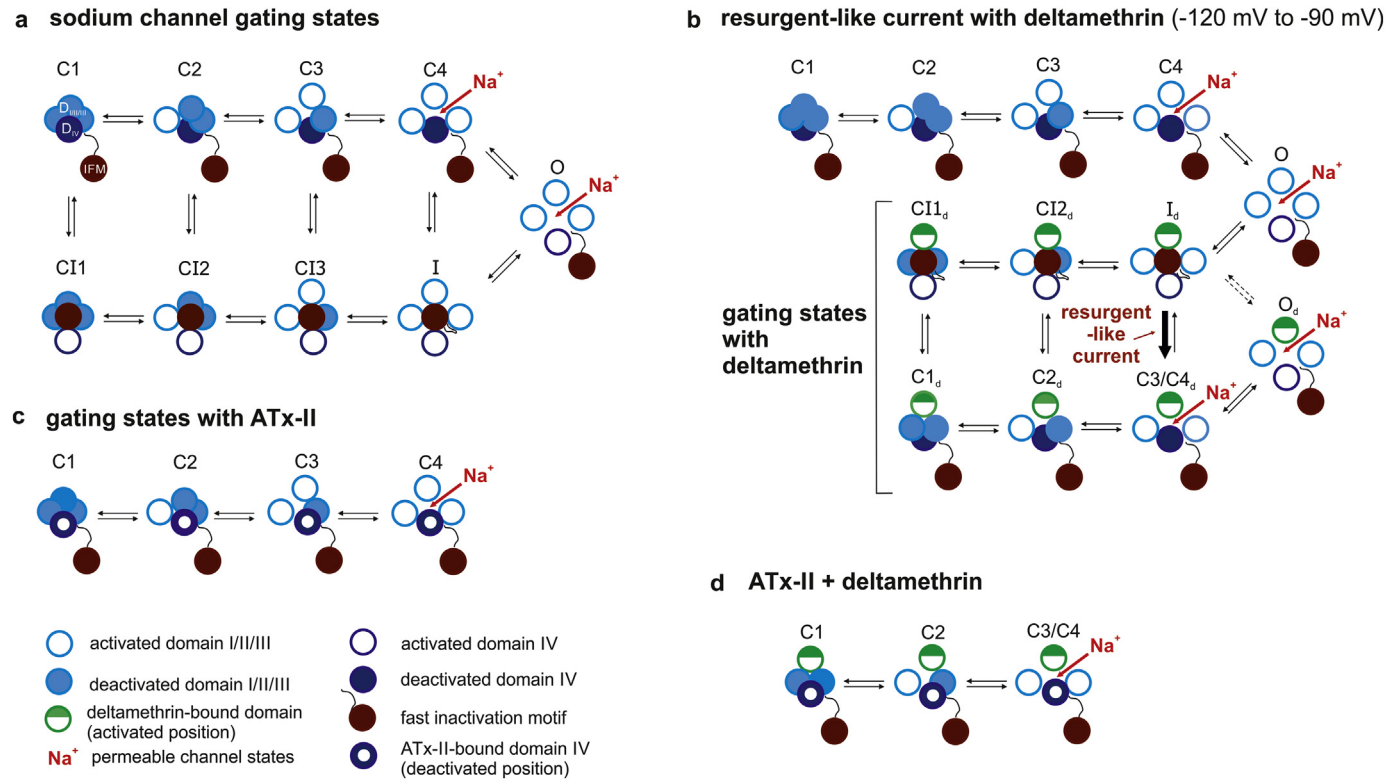

Fig. 7. Deltamethrin produces resurgent-like currents by slowing deactivation.
(a) Schematic display of gating states of human Nav1.5 channels. During activation, channels transition between closed states C1 to C4 with DI-III moving outward fast (unfilled light blue). Following activation, channels are permeable either with DIV still deactivated (filled dark blue) in state C4 or with DI-IV completely activated in state O. When DIV is activated (unfilled dark blue), channels quickly undergo fast inactivation and the inactivation particle (IFM, filled red) occludes the open pore (I). Upon repolarization with the inactivation particle bound, DI-III deactivate fast (filled light blue) (CI3-CI1). Accompanying the deactivation of DIV, the inactivation particle unbinds from the pore, returning the channel to state C1. (b) Schematic display of gating states of Nav1.5 channels treated by deltamethrin and producing resurgent-like currents. We propose that resurgent-like currents only occur in channels that bind deltamethrin after having undergone fast inactivation. Therefore, the first gating states that occur during channel activation (C1-C4-O) are analogous to (a). Once the inactivated channel has bound deltamethrin (I_d), DII (white-green) is stabilized in its activated position. Thus, gating states C3 and C4 become identical and permeable ($C3/C4_d$). Bold arrow indicates the transition that may lead to resurgent-like currents: As deltamethrin slows channel deactivation, recovery from fast inactivation (I_d-$C3/C4_d$) may precede deactivation and briefly return the channel to a conductive state. Fast inactivation of deltamethrin-bound channels (O_d-I_d) is slowed (dashed arrows), leading to large persistent currents. (c) Schematic display of gating states of Nav1.5 channels treated by ATx-II. Activation of DIV (open dark blue) is inhibited, preventing the binding of the fast inactivation particle to the open channel pore. Only gating state C4 is therefore conductive. In this theoretical model, states O, I and CI do not exist. (d) Schematic display of gating states of Nav1.5 channels treated by ATx-II and deltamethrin. DII (white-green) is stabilized in its activated position by deltamethrin as in (b). Activation of DIV (open dark blue) is inhibited by ATx-II and prevents fast inactivation as in (c). C3/C4 is permeable. In this theoretical model, states O, I and CI do not exist. In this simplified overview, possible additional states and transitions between depicted states are not captured but may occur. Channel states: C closed, O open, I inactivated, CI closed-inactivated; a subscript $_d$ indicates a deltamethrin-bound state. See main text for further details. (For interpretation of the references to colour in this figure legend, the reader is referred to the web version of this article.)

kinetics, producing large persistent currents.

4.2. Hooked, resurgent-like currents

To date the induction of resurgent currents has been believed to require the presence of an open-channel blocker, such as the short cytoplasmic C-terminus of the sodium channel β4-subunit (Grieco et al., 2005). This peptide contains positively charged residues and is supposed to block open sodium channels from the intracellular side at positive voltages and unblock at negative potentials, while competing with fast inactivation (Lewis and Raman, 2014).

Contrary to the previously known β4-peptide-induced resurgent currents, which occur at repolarizing voltages ranging from −70 mV to −30 mV, deltamethrin surprisingly produced hooked, resurgent-like currents at very negative potentials (−120 mV to −90 mV) (Fig. 2b). However, deltamethrin is not polar, unlike the β4-peptide, whose polarity is believed to be crucial for open-channel block (Grieco et al., 2005; Lewis and Raman, 2011). Instead lipophilic pyrethroids are predicted to bind at a lipid-accessible transmembrane site on Nav channels (O'Reilly et al., 2006). This implies that deltamethrin induces hooked, resurgent-like currents by a distinct mechanism.

Generally, with deltamethrin binding to the channel at rest or during activation, two fractions of channels can be observed: a deltamethrin-bound fraction that produces large persistent currents (Fig. 4) (James et al., 2017), and an unbound fraction that undergoes regular channel gating. The latter displays an unaffected voltage dependence of activation and steady-state fast inactivation as well as unchanged time constants of fast inactivation and deactivation.

We propose that hooked, resurgent-like currents are generated by a third, very small fraction of channels that bind deltamethrin *after* they have undergone fast inactivation (Fig. 7b): At very hyperpolarized potentials, the deactivation of DI-IV proceeds very quickly (Kuo and Bean, 1994; Armstrong, 2006; Lewis and Raman, 2014). Deltamethrin keeps DII in its activated position (Fig. 7b), and thereby slows deactivation. In parallel, the channel will recover from fast inactivation at these negative potentials, which is mainly mediated by DIV movement to its deactivated position. Deactivation of DIV is believed to be rate-limiting for the inactivation particle to unbind from the channel pore (Kuo and Bean, 1994; Armstrong, 2006; Capes et al., 2013; Goldschen-Ohm et al., 2013; Ahern et al., 2016). With DII remaining in its outward position, recovery of fast inactivation becomes faster than deactivation of DII. If DIV recovers before any of the other three domains, then the inactivation particle will unbind before the channel is fully closed by deactivation. The channel will therefore become conductive at these negative potentials (Fig. 7b, I_d – $C3/C4_d$; bold arrow), resulting in hooked, resurgent-like currents. If DI or DIII deactivate before DIV (Fig. 7b, transition $CI2_d$ – $C2_d$ or $CI1_d$ – $C1_d$), no resurgent-like current can occur since a minimum of three domains has to be in the activated position for the channel to be conductive (Armstrong, 2006).

At more positive repolarization voltages, fast inactivation is favored and recovery from fast inactivation occurs slower. This would reduce the likelihood of DIV to deactivate before DI or DIII and channels therefore remain blocked by the inactivation particle until at least two channel domains return to their resting states (Kuo and Bean, 1994; Armstrong, 2006; Lewis and Raman, 2014). Under these circumstances, deltamethrin would not be able to induce resurgent-like currents at more positive voltages. These findings correspond well with our conclusion that resurgent-like currents may arise when movement of at least one of the Nav channel domains I, II or III is altered.

4.3. Additional permeable Nav channel gating states

The finding that deltamethrin renders Nav channels conductive during hyperpolarized potentials and induces hooked, resurgent-like currents without an additional open-channel blocker, confirms two conclusions: First, DIV is able to deactivate before DI, DII and DIII. Second, channels with deactivated DIV are permeable to sodium current when recovery of fast inactivation happens before the other three domains are deactivated (Armstrong, 2006). Accordingly, Nav channels have to have more than only one conductive state, thus they can generate resurgent-like currents.

With deltamethrin stabilizing the activated DII, the total number of channel states in our simplified model is reduced from nine to seven (compare Fig. 7a to lower part of Fig. 7b). Thus, with deltamethrin the $C3/C4_d$ state is reached quicker as there are only two closed states that precede this conductive state (Fig. 7b) and the probability to switch into one of the conductive states is increased. This is reflected in a slight shift of voltage dependence of activation to more hyperpolarized potentials by deltamethrin (Fig. 4b).

4.4. ATx-II confirms additional permeable gating states

ATx-II is thought to stabilize DIV in its deactivated conformation (Sheets et al., 1999; Stevens et al., 2011), impairing open-state fast inactivation (Warmke et al., 1997; Vais et al., 2000). Closed-state inactivation was first thought to be only marginally affected (el-Sherif et al., 1992). Yet, later results have shown that ATx-II strongly impairs closed-state inactivation (Warmke et al., 1997).

Accordingly, by preventing DIV from activating and thus preventing the inactivation particle from occluding the channel pore (Vais et al., 2000; Lewis and Raman, 2013), the amount of permeable channel states is reduced to one (Fig. 7c). At the same time, closed-inactivated (CI) states, with the fast inactivation particle blocking the channel pore, do not exist in this theoretical model. A fully activated state (O) also does not exist, as DIV cannot activate. Accordingly, the only conductive state is C4.

When ATx-II and deltamethrin are applied at the same time, the number of total channel states is further reduced to three as C3 and C4 again become equivalent (Fig. 7d). The number of conducting states remains one (C3/C4). This is in contrast to the situation with deltamethrin alone (Fig. 7b), where there are two conducting states ($C3/C4_d$ and O_d).

ATx-II completely eliminated resurgent-like currents in Nav1.5 channels treated by deltamethrin. This may have two reasons: binding of ATx-II and deltamethrin inhibit each other, or resurgent-like currents depend on channel inactivation, which is abolished by ATx-II. While it is unlikely that the binding of ATx-II prohibits additional binding of deltamethrin due to different binding sites (Rogers et al., 1996; Vais et al., 2003; O'Reilly et al., 2014), we cannot fully exclude this possibility. However, persistent currents during ATx-II plus deltamethrin treatment showed the same voltage dependence as those with deltamethrin alone but different to those mediated by ATx-II with β4-peptide (see Fig. 3c (Thull et al., 2020)). Additionally, Nav channels affected by the triple combination of ATx-II, β4-peptide and deltamethrin present resurgent currents occurring from −120 mV to −10 mV (see Fig. 3e (Thull et al., 2020)), which can only be explained by different binding sites and synergistically working mechanisms of all three substances.

Since resurgent-like currents do not occur with ATx-II and since ATx-II prevents DIV activation, it can be assumed that the movement of DIV is essential for hooked, resurgent-like currents. Following this interpretation and our recent results, we can assume that with ATx-II and deltamethrin, the inactivation particle does not bind to the channel pore (Fig. 7c, d) and therefore cannot unbind to allow resurgent-like current. Thus, if ATx-II and deltamethrin are present, slowing of deactivation of DII by deltamethrin does not suffice to produce resurgent-like currents.

4.5. Physiological relevance

A similar connection between recovery of fast inactivation through conductive channel states and resurgent-like currents has been hypothesized earlier, with the observation of analogous currents induced

by the pyrethroid tetramethrin in rat Purkinje cells and dorsal root ganglia. These currents have been described as “hooked tail currents” (Tatebayashi and Narahashi, 1994; Song and Narahashi, 1996). They have also been observed in adult frog muscle (Leibowitz et al., 1987) and were linked to a β-scorpion toxin-induced negative-shift in activation of DIS4, DIIS4 and DIIIS4 of different Nav channel types (Cestèle et al., 1998; Schiavon et al., 2006, 2012). By deconstructing the different Nav channel states contributing to hooked, resurgent-like currents induced by deltamethrin in fast gating Nav1.5 channels, our results generally confirm this alternative mechanism of resurgent current generation. These resurgent-like currents are primarily known to be caused by toxins that slow the deactivation of Nav channel domain I, II or III.

Importantly, long-term studies have revealed that environmental exposure to pyrethroid insecticdes is linked to an increased risk of coronary heart disease and cardiovascular disease mortality (Han et al., 2017; Bao et al., 2019). Accordingly, reports exist of chest tightness and palpitations after deltamethrin intoxication (He et al., 1989; Mowry et al., 2016). Our data generally support the notion of cardiac side effects due to deltamethrin and we provide a detailed investigation of the compound's effects on human cardiac Nav1.5 channels.

Following occupational dermal exposure, main adverse effects are paranesthesiae, most likely due to hyperactivity of cutaneous sensory nerve fibres (Bradberry et al., 2005). Main symptoms of pyrethroid poisoning are neurological since pyrethroids are known to pass through the blood-brain barrier due to their lipohilicity (Bradberry et al., 2005; Godin et al., 2010). However, plasma protein binding limits brain uptake of deltamethrin under physiological conditions, which adds further evidence to the low acute CNS toxicity in humans in non-excessive exposures (Amaraneni et al., 2016), although chronic long-term pyrethroid exposure seems to be associated with neurological deficits such as deteriorated neurocognitive performance (Hansen et al., 2017). Hooked tail currents are not only present in cardiac Nav1.5 channels but also in neuronal Nav channels such as Nav1.7 and Nav1.8. Deltamethrin also affects β4-mediated “conventional” resurgent currents. The combination of β4-peptide and deltamethrin involves two mechanisms working synergistically to produce enhanced, voltage-independent resurgent currents: As deltamethrin is believed to stabilize the opened Nav channel pore, it facilitates the β4-peptide to find its way into the channel pore, even at very negative potentials. Thus, intoxication effects mediated by neuronal Nav channels subtypes might be aggravated by these two synergistically working mechanisms. Consequently, deltamethrin might also have an impact on the firing behavior of cell types naturally producing resurgent currents such as purkinje cells (Raman and Bean, 1997, 2001), in addition to the obvious, large persistent current induced by the compound.

Thus, we here uncovered the mechanism underlying those resurgent-like currents exemplarily in Nav1.5 channels. Further investigations about resurgent-like currents in other neuronal Nav channel subtypes such as Nav1.9 and their impact on Nav channel gating properties are essential and beneficial to fully understand the pyrethroids' effect on neuronal Nav channel subtypes, causing the prominent and severe neuronal intoxication symptoms.

5. Conclusion

In summary, our data show that deltamethrin, a type-II pyrethroid, can induce hooked, resurgent-like currents in the absence of a pore-blocker in human cardiac Nav1.5 channels. These currents are generated by re-opening Nav1.5 channels, when they recover from fast inactivation before they completely deactivate. By establishing a model of ATx-II and deltamethrin interaction with Nav channels, we show that resurgent currents can be induced by slowing deactivation and thus by disrupting the interaction between fast inactivation and deactivation of Nav channels. Our findings highlight how Nav channel functions can be affected by even small disruptions of the sensitive interplay of their different gating states. Our investigations of deltamethrin in human cardiac Nav1.5 channels characterize potential effects of pyrethroid exposure for humans and can provide a first attempt in explaining cardiac symptoms induced by deltamethrin. Since pyrethroids are very common insecticides, our results emphasize the importance of investigating their broad spectrum of effects on human Nav channels in detail.

Related article

Sarah Thull, Cristian Neacsu, Andrias O. O'Reilly, Stefanie Bothe, Ralf Hausmann, Tobias Huth, Jannis Meents, Angelika Lampert. Dataset of electrophysiological patch-clamp recordings of the effect of the compounds deltamethrin, ATx-II and β4-peptide on human cardiac Nav1.5 channel gating properties. 2020. *Data in Brief*.

Declaration of Competing Interest

None.

Acknowledgements

The authors thank Petra Hautvast and Brigitte Hoch for excellent technical assistance. The authors declare no competing financial interests. This work was supported in part by the DFG LA2740/3-1 and the DFG-funded research training groups363055819/GRK2415 and 368482240/GRK2416 (all to A.L.).

References

el-Sherif, N., Fozzard, H.A., Hanck, D.A., 1992. Dose-dependent modulation of the cardiac sodium channel by sea anemone toxin ATXII. Circ. Res. 70, 285–301. https://doi.org/10.1161/01.RES.70.2.285.

Ahern, C.A., 2013. What activates inactivation? J. Gen. Physiol. 142, 97–100. https://doi.org/10.1085/jgp.201311046.

Ahern, C.A., Payandeh, J., Bosmans, F., Chanda, B., 2016. The hitchhiker's guide to the voltage-gated sodium channel galaxy. J. Gen. Physiol. 147, 1–24. https://doi.org/10.1085/jgp.201511492.

Amaraneni, M., Sharma, A., Pang, J., Muralidhara, S., Cummings, B.S., White, C.A., Bruckner, J.V., Zastre, J., 2016. Plasma protein binding limits the blood brain barrier permeation of the pyrethroid insecticide, deltamethrin. Toxicol. Lett. 250–251, 21–28. https://doi.org/10.1016/j.toxlet.2016.03.006.

Armstrong, C.M., 1981. Sodium channels and gating currents. Physiol. Rev. 61, 644–683.

Armstrong, C.M., 2006. Na channel inactivation from open and closed states. Proc. Natl. Acad. Sci. U. S. A. 103, 17991–17996. https://doi.org/10.1073/pnas.0607603103.

Bao, W., Liu, B., Simonsen, D.W., Lehmler, H.-J., 2019. Association between exposure to pyrethroid insecticides and risk of all-cause and cause-specific mortality in the general US adult population. JAMA Intern. Med. https://doi.org/10.1001/jamainternmed.2019.6019.

Bezanilla, F., Armstrong, C., 1977. Inactivation of the sodium channel. I. Sodium current experiments. J. Gen. Physiol. 70, 549–566.

Bradberry, S.M., Cage, S.A., Proudfoot, A.T., Vale, J.A., 2005. Poisoning due to pyrethroids. Toxicol. Rev. 24, 93–106. https://doi.org/10.2165/00139709-200524020-00003.

Calhoun, J.D., Isom, L.L., 2014. The role of non-pore-forming β subunits in physiology and pathophysiology of voltage-gated sodium channels. Handb. Exp. Pharmacol. 221, 51–89. https://doi.org/10.1007/978-3-642-41588-3_4.

Capes, D.L., Goldschen-Ohm, M.P., Arcisio-Miranda, M., Bezanilla, F., Chanda, B., 2013. Domain IV voltage-sensor movement is both sufficient and rate limiting for fast inactivation in sodium channels. J. Gen. Physiol. 142, 101–112. https://doi.org/10.1085/jgp.201310998.

Catterall, W.A., 2000. From ionic currents to molecular mechanisms: the structure and function of voltage-gated sodium channels. Neuron 26, 13–25.

Catterall, W.A., 2010. Ion Channel voltage sensors: structure, function, and pathophysiology. Neuron 67, 915–928. https://doi.org/10.1016/j.neuron.2010.08.021.

Cestèle, S., Qu, Y., Rogers, J.C., Rochat, H., Scheuer, T., Catterall, W.A., 1998. Voltage sensor-trapping: enhanced activation of sodium channels by beta-scorpion toxin bound to the S3-S4 loop in domain II. Neuron 21, 919–931.

Chahine, M., George, A.L., Zhou, M., Ji, S., Sun, W., Barchi, R.L., Horn, R., 1994. Sodium channel mutations in paramyotonia congenita uncouple inactivation from activation. Neuron 12, 281–294. https://doi.org/10.1016/0896-6273(94)90271-2.

Chanda, B., Bezanilla, F., 2002. Tracking voltage-dependent conformational changes in skeletal muscle sodium channel during activation. J. Gen. Physiol. 120, 629–645.

Chinn, K., Narahashi, T., 1986. Stabilization of sodium channel states by deltamethrin in mouse neuroblastoma cells. J. Physiol. 380, 191–207. https://doi.org/10.1113/jphysiol.1986.sp016280.

Dong, K., Du, Y., Rinkevich, F., Nomura, Y., Xu, P., Wang, L., Silver, K., Zhorov, B.S., 2014. Molecular biology of insect sodium channels and Pyrethroid resistance. Insect Biochem. Mol. Biol. 50, 1–17. https://doi.org/10.1016/j.ibmb.2014.03.012.

Du, Y., Nomura, Y., Zhorov, B.S., Dong, K., 2015. Evidence for dual binding sites for DDT in insect sodium channels. J. Biol. Chem. https://doi.org/10.1074/jbc.M115.678672.

Field, L.M., Emyr Davies, T.G., O'Reilly, A.O., Williamson, M.S., Wallace, B.A., 2017. Voltage-gated sodium channels as targets for pyrethroid insecticides. Eur. Biophys. J. 46, 675–679. https://doi.org/10.1007/s00249-016-1195-1.

Godin, S.J., DeVito, M.J., Hughes, M.F., Ross, D.G., Scollon, E.J., Starr, J.M., Setzer, R.W., Conolly, R.B., Tornero-Velez, R., 2010. Physiologically based pharmacokinetic modeling of deltamethrin: development of a rat and human diffusion-limited model. Toxicol. Sci. Off. J. Soc. Toxicol. 115, 330–343. https://doi.org/10.1093/toxsci/kfq051.

Goldschen-Ohm, M.P., Capes, D.L., Oelstrom, K.M., Chanda, B., 2013. Multiple pore conformations driven by asynchronous movements of voltage sensors in a eukaryotic sodium channel. Nat. Commun. 4, 1350. https://doi.org/10.1038/ncomms2356.

Grieco, T.M., Malhotra, J.D., Chen, C., Isom, L.L., Raman, I.M., 2005. Open-channel block by the cytoplasmic tail of sodium channel beta4 as a mechanism for resurgent sodium current. Neuron 45, 233–244. https://doi.org/10.1016/j.neuron.2004.12.035.

Hampl, M., Eberhardt, E., O'Reilly, A.O., Lampert, A., 2016. Sodium channel slow inactivation interferes with open channel block. Sci. Rep. 6, 25974. https://doi.org/10.1038/srep25974.

Han, J., Zhou, L., Luo, M., Liang, Y., Zhao, W., Wang, P., Zhou, Z., Liu, D., 2017. Nonoccupational exposure to pyrethroids and risk of coronary heart disease in the Chinese population. Environ. Sci. Technol. 51, 664–670. https://doi.org/10.1021/acs.est.6b05639.

Hansen, M.R.H., Jørs, E., Lander, F., Condarco, G., Debes, F., Tirado Bustillos, N., Schlünssen, V., 2017. Neurological deficits after long-term pyrethroid exposure. Environ. Health Insights. 11. https://doi.org/10.1177/1178630217700628.

Hargus, N.J., Nigam, A., Bertram, E.H., Patel, M.K., 2013. Evidence for a role of Nav1.6 in facilitating increases in neuronal hyperexcitability during epileptogenesis. J. Neurophysiol. 110, 1144–1157. https://doi.org/10.1152/jn.00383.2013.

He, B., Soderlund, D.M., 2016. Effects of the β1 auxiliary subunit on modification of rat Nav1.6 sodium channels expressed in HEK293 cells by the pyrethroid insecticides tefluthrin and deltamethrin. Toxicol. Appl. Pharmacol. 291, 58–69. https://doi.org/10.1016/j.taap.2015.12.007.

He, F., Wang, S., Liu, L., Chen, S., Zhang, Z., Sun, J., 1989. Clinical manifestations and diagnosis of acute pyrethroid poisoning. Arch. Toxicol. 63, 54–58.

James, T.F., Nenov, M.N., Tapia, C.M., Lecchi, M., Koshy, S., Green, T.A., Laezza, F., 2017. Consequences of acute Nav1.1 exposure to deltamethrin. Neurotoxicology 60, 150–160. https://doi.org/10.1016/j.neuro.2016.12.005.

Jarecki, B.W., Piekarz, A.D., Jackson, J.O., Cummins, T.R., 2010. Human voltage-gated sodium channel mutations that cause inherited neuronal and muscle channelopathies increase resurgent sodium currents. J. Clin. Invest. 120, 369–378. https://doi.org/10.1172/JCI40801.

Kaluza, L., Meents, J.E., Hampl, M., Rösseler, C., Hautvast, P.A.I., Detro-Dassen, S., Hausmann, R., Schmalzing, G., Lampert, A., 2018. Loss-of-function of Nav1.8/D1639N linked to human pain can be rescued by lidocaine. Pflüg. Arch. Eur. J. Physiol. 470, 1787–1801. https://doi.org/10.1007/s00424-018-2189-x.

Klinger, A.B., Eberhardt, M., Link, A.S., Namer, B., Kutsche, L.K., Schuy, E.T., Sittl, R., Hoffmann, T., Alzheimer, C., Huth, T., Carr, R.W., Lampert, A., 2012. Sea-anemone toxin ATX-II elicits a-fiber-dependent pain and enhances resurgent and persistent sodium currents in large sensory neurons. Mol. Pain 8, 69. https://doi.org/10.1186/1744-8069-8-69.

Klugbauer, N., Lacinova, L., Flockerzi, V., Hofmann, F., 1995. Structure and functional expression of a new member of the tetrodotoxin-sensitive voltage-activated sodium channel family from human neuroendocrine cells. EMBO J. 14, 1084–1090.

Kuo, C.-C., Bean, B.P., 1994. Na+ channels must deactivate to recover from inactivation. Neuron 12, 819–829. https://doi.org/10.1016/0896-6273(94)90335-2.

Leibowitz, M.D., Schwarz, J.R., Holan, G., Hille, B., 1987. Electrophysiological comparison of insecticide and alkaloid agonists of Na channels. J. Gen. Physiol. 90, 75–93.

Lewis, A.H., Raman, I.M., 2011. Cross-species conservation of open-channel block by Na channel β4 peptides reveals structural features required for resurgent Na current. J. Neurosci. 31, 11527–11536. https://doi.org/10.1523/JNEUROSCI.1428-11.2011.

Lewis, A.H., Raman, I.M., 2013. Interactions among DIV voltage-sensor movement, fast inactivation, and resurgent Na current induced by the NaVβ4 open-channel blocking peptide. J. Gen. Physiol. 142, 191–206. https://doi.org/10.1085/jgp.201310984.

Lewis, A.H., Raman, I.M., 2014. Resurgent current of voltage-gated Na(+) channels. J. Physiol. 592, 4825–4838. https://doi.org/10.1113/jphysiol.2014.277582.

McCavera, S.J., Soderlund, D.M., 2012. Differential state-dependent modification of inactivation-deficient Nav1.6 sodium channels by the pyrethroid insecticides S-bioallethrin, tefluthrin and deltamethrin. Neurotoxicology 33, 384–390. https://doi.org/10.1016/j.neuro.2012.03.007.

Meents, et al., 2018. The opioid oxycodone use-dependently inhibits the cardiac sodium channel Na_V 1.5. British Journal of Pharmacology 175 (14). https://doi.org/10.1111/bph.14348.

Mowry, J.B., Spyker, D.A., Brooks, D.E., Zimmerman, A., Schauben, J.L., 2016. 2015 annual report of the American association of poison control centers' national poison data system (NPDS): 33rd annual report. Clin. Toxicol. Phila. Pa. 54, 924–1109. https://doi.org/10.1080/15563650.2016.1245421.

O'Reilly, A.O., Khambay, B.P.S., Williamson, M.S., Field, L.M., WAllace, B.A., Davies, T.G.E., 2006. Modelling insecticide-binding sites in the voltage-gated sodium channel. Biochem. J. 396, 255–263. https://doi.org/10.1042/BJ20051925.

O'Reilly, A.O., Williamson, M.S., González-Cabrera, J., Turberg, A., Field, L.M., Wallace, B.A., Davies, T.G.E., 2014. Predictive 3D modelling of the interactions of pyrethroids with the voltage-gated sodium channels of ticks and mites. Pest Manag. Sci. 70, 369–377. https://doi.org/10.1002/ps.3561.

Oliveira, E.E., Du, Y., Nomura, Y., Dong, K., 2013. A residue in the transmembrane segment 6 of domain I in insect and mammalian sodium channels regulate differential sensitivities to pyrethroid insecticides. Neurotoxicology 38, 42–50. https://doi.org/10.1016/j.neuro.2013.06.001.

Pan, X., Li, Z., Zhou, Q., Shen, H., Wu, K., Huang, X., Chen, J., Zhang, J., Zhu, X., Lei, J., Xiong, W., Gong, H., Xiao, B., Yan, N., 2018. Structure of the human voltage-gated sodium channel Nav1.4 in complex with β1. Science 362https://doi.org/10.1126/science.aau2486. eaau2486.

Raman, I.M., Bean, B.P., 1997. Resurgent sodium current and action potential formation in dissociated cerebellar purkinje neurons. J. Neurosci. 17, 4517–4526.

Raman, I.M., Bean, B.P., 2001. Inactivation and recovery of sodium currents in cerebellar purkinje neurons: evidence for two mechanisms. Biophys. J. 80, 729–737.

Rogers, J.C., Qu, Y., Tanada, T.N., Scheuer, T., Catterall, W.A., 1996. Molecular determinants of high affinity binding of alpha-scorpion toxin and sea anemone toxin in the S3-S4 extracellular loop in domain IV of the Na+ channel alpha subunit. J. Biol. Chem. 271, 15950–15962.

Rühlmann, A.H., Körner, J., Bebrivenski, N., Detro-Dassen, S., Hautvast, P., Benasolo, C.A., Meents, J., Machtens, J.-P., Schmalzing, G., Lampert, A., 2019. Uncoupling sodium channel dimers rescues phenotype of pain-linked Nav1.7 mutation. Biorxiv 716654. https://doi.org/10.1101/716654.

Schiavon, E., Sacco, T., Cassulini, R.R., Gurrola, G., Tempia, F., Possani, L.D., Wanke, E., 2006. Resurgent current and voltage sensor trapping enhanced activation by a beta-scorpion toxin solely in Nav1.6 channel. Significance in mice purkinje neurons. J. Biol. Chem. 281, 20326–20337. https://doi.org/10.1074/jbc.M600565200.

Schiavon, E., Pedraza-Escalona, M., Gurrola, G.B., Olamendi-Portugal, T., Corzo, G., Wanke, E., Possani, L.D., 2012. Negative-shift activation, current reduction and resurgent currents induced by β-toxins from centruroides scorpions in sodium channels. Toxicon Off. J. Int. Soc. Toxinology. 59, 283–293. https://doi.org/10.1016/j.toxicon.2011.12.003.

Sheets, M.F., Kyle, J.W., Kallen, R.G., Hanck, D.A., 1999. The Na channel voltage sensor associated with inactivation is localized to the external charged residues of domain IV, S4. Biophys. J. 77, 747–757. https://doi.org/10.1016/S0006-3495(99)76929-8.

Soderlund, D.M., 2010. State-dependent modification of voltage-gated sodium channels by pyrethroids. Pestic. Biochem. Physiol. 97, 78–86. https://doi.org/10.1016/j.pestbp.2009.06.010.

Soderlund, D.M., 2012. Molecular mechanisms of pyrethroid insecticide neurotoxicity: recent advances. Arch. Toxicol. 86, 165–181. https://doi.org/10.1007/s00204-011-0726-x.

Song, J.H., Narahashi, T., 1996. Modulation of sodium channels of rat cerebellar purkinje neurons by the pyrethroid tetramethrin. J. Pharmacol. Exp. Ther. 277, 445–453.

Stadler, T., O'Reilly, A.O., Lampert, A., 2015. Erythromelalgia mutation Q875E stabilizes the activated state of sodium channel Nav1.7. J. Biol. Chem. 290, 6316–6325. https://doi.org/10.1074/jbc.M114.605899.

Stevens, M., Peigneur, S., Tytgat, J., 2011. Neurotoxins and their binding areas on voltage-gated sodium channels. Front. Pharmacol. 2. https://doi.org/10.3389/fphar.2011.00071.

Tabarean, I.V., Narahashi, T., 1998. Potent modulation of tetrodotoxin-sensitive and tetrodotoxin-resistant sodium channels by the type II pyrethroid deltamethrin. J. Pharmacol. Exp. Ther. 284, 958–965.

Tabarean, I.V., Narahashi, T., 2001. Kinetics of modulation of tetrodotoxin-sensitive and tetrodotoxin-resistant sodium channels by tetramethrin and deltamethrin. J. Pharmacol. Exp. Ther. 299, 988–997.

Tan, J., Soderlund, D.M., 2010. Divergent actions of the pyrethroid insecticides s-bioallethrin, tefluthrin and deltamethrin on rat Nav1.6 sodium channels. Toxicol. Appl. Pharmacol. 247, 229–237. https://doi.org/10.1016/j.taap.2010.07.001.

Tan, J., Soderlund, D.M., 2011. Actions of tefluthrin on rat Nav1.7 voltage-gated sodium channels expressed in xenopus oocytes. Pestic. Biochem. Physiol. 101, 21–26. https://doi.org/10.1016/j.pestbp.2011.06.001.

Tatebayashi, H., Narahashi, T., 1994. Differential mechanism of action of the pyrethroid tetramethrin on tetrodotoxin-sensitive and tetrodotoxin-resistant sodium channels. J. Pharmacol. Exp. Ther. 270, 595–603.

Thull, S., Neacsu, C., O'Reilly, A.O., Bothe, S., Hausmann, R., Huth, T., Meents, J., Lampert, A., 2020. Dataset of electrophysiological patch-clamp recordings of the effect of the compounds deltamethrin, ATx-II and β4-peptide on human cardiac Nav1.5 channel gating properties. In: Data in Brief, Under review.

Usherwood, P.N.R., Davies, T.G.E., Mellor, I.R., O'Reilly, A.O., Peng, F., Vais, H., Khambay, B.P.S., Field, L.M., Williamson, M.S., 2007. Mutations in DIIS5 and the DIIS4-S5 linker of drosophila melanogaster sodium channel define binding domains for pyrethroids and DDT. FEBS Lett. 581, 5485–5492. https://doi.org/10.1016/j.febslet.2007.10.057.

Vais, H., Williamson, M.S., Goodson, S.J., Devonshire, A.L., Warmke, J.W., Usherwood, P.N., Cohen, C.J., 2000. Activation of Drosophila sodium channels promotes modification by deltamethrin. Reductions in affinity caused by knock-down resistance mutations. J. Gen. Physiol. 115, 305–318.

Vais, H., Atkinson, S., Pluteanu, F., Goodson, S.J., Devonshire, A.L., Williamson, M.S., Usherwood, P.N.R., 2003. Mutations of the para sodium channel of drosophila melanogaster identify putative binding sites for pyrethroids. Mol. Pharmacol. 64, 914–922. https://doi.org/10.1124/mol.64.4.914.

Varga, Z., Zhu, W., Schubert, A.R., Pardieck, J.L., Krumholz, A., Hsu, E.J., Zaydman, M.A., Cui, J., Silva, J.R., 2015. Direct measurement of cardiac Na+ channel conformations reveals molecular pathologies of inherited mutations. Circ. Arrhythm. Electrophysiol. 8, 1228–1239. https://doi.org/10.1161/CIRCEP.115.003155.

Warmke, J.W., Reenan, R.A.G., Wang, P., Qian, S., Arena, J.P., Wang, J., Wunderler, D., Liu, K., Kaczorowski, G.J., der Ploeg, L.H.T.V., Ganetzky, B., Cohen, C.J., 1997. Functional expression of drosophila para sodium channels : modulation by the

membrane protein TipE and toxin pharmacology. J. Gen. Physiol. 110, 119–133. https://doi.org/10.1085/jgp.110.2.119.
West, J.W., Patton, D.E., Scheuer, T., Wang, Y., Goldin, A.L., Catterall, W.A., 1992. A cluster of hydrophobic amino acid residues required for fast Na(+)-channel inactivation. Proc. Natl. Acad. Sci. U. S. A. 89, 10910–10914.
Xiao, Y., Blumenthal, K., Cummins, T.R., 2014. Gating-pore currents demonstrate selective and specific modulation of individual sodium channel voltage-sensors by biological toxins. Mol. Pharmacol. 86, 159–167. https://doi.org/10.1124/mol.114.092338.
Yan, Z., Zhou, Q., Wang, L., Wu, J., Zhao, Y., Huang, G., Peng, W., Shen, H., Lei, J., Yan, N., 2017. Structure of the Nav1.4-β1 complex from electric eel. Cell 170, 470–482. e11. https://doi.org/10.1016/j.cell.2017.06.039.
Yang, N., George, A.L., Horn, R., 1996. Molecular basis of charge movement in voltage-gated sodium channels. Neuron 16, 113–122. https://doi.org/10.1016/S0896-6273(00)80028-8.
Zaydman, M.A., Silva, J.R., Cui, J., 2012. Ion channel associated diseases: overview of molecular mechanisms. Chem. Rev. 112, 6319–6333. https://doi.org/10.1021/cr300360k.
Zhu, W., Voelker, T.L., Varga, Z., Schubert, A.R., Nerbonne, J.M., Silva, J.R., 2017. Mechanisms of noncovalent β subunit regulation of NaV channel gating. J. Gen. Physiol. https://doi.org/10.1085/jgp.201711802.